Terahertz Active and Passive Imaging

E. N. Grossman[1], J. Gordon[1], D. Novotny[1], and R. Chamberlin[2]
[1] Physical Measurement Laboratory, Natl. Inst. Of Standards and Technology, Boulder, CO United States
[2] University of Colorado, Dept. of Electrical Engineering, Boulder, CO
erich.grossman@nist.gov

***Abstract*—We describe the results of bistatic scattering measurements covering 325-650 GHz on a series of well-characterized random rough test surfaces. These have implications for active THz imagers that use coherent sources for illumination. The mean scattered intensity is compared to theoretical predictions based on an integral equation method, and the fluctuations are examined in terms of the theory for fully developed speckle. We also present a preliminary, fully passive image made using a recently developed 650 GHz, InP HEMT low-noise amplifier, and compare it to a very similar passive image made using a cryogenic (4K) hotspot microbolometer.**

***Index Terms*—antenna, propagation, measurement, terahertz, submillimeter, passive, imaging**

I. Introduction

Terahertz technology, here encompassing a frequency range from 0.3 to 10 THz (wavelengths 0.03 - 1 mm), has grown dramatically in the last decade, to the point that attempting any overview of the entire field, along the lines of [1] (written in 2002) would be a fool's errand. The inaugural issue of the IEEE Trans. on THz Science and Technology contains several review articles on important subfields, including some that relate to THz imaging for particular applications[2-4]. The present paper briefly describes work recently conducted at NIST that directly relates to THz imaging in "real-world" applications. Specifically, this means that the samples being imaged are in their natural state, not artificially smoothed, and that the imaging systems are meant to be operated in ordinary environments, not in laboratories.

Among THz imagers, one commonly distinguishes between passive systems, that record the contrast in radiometric temperature within a scene, and active systems that record the contrast in (some property of) the scattered radiance within a scene when it is illuminated with some type of THz source. Further, one commonly subdivides active systems into those with ranging capability (i.e. radars) and those without it. The latter generally record the total intensity of the scattered radiance, and are termed (in this paper) amplitude-only, active imagers. The great advantage of any active imager, whether ranging or not, is the fact that active illumination greatly reduces the sensitivity requirement on the THz receivers. Many of the most practical imagers developed to date (see Table I) rely on this advantage, by trading receiver sensitivity for other practical benefits such as acquisition speed, format (i.e. number of image pixels), and cost. In terms of image interpretation however, it is not so clear whether the advantage lies with active or passive systems.

In this paper we first discuss two subjects related to the phenomenology of amplitude-only active imaging: the non-Lambertian (angular) reflectance distribution of real surfaces, and the influence of THz speckle in active images of such surfaces when the illumination is coherent. Then, we describe some initial passive imaging experiments made using recently developed, uncooled 650 GHz amplifiers. The noise performance of these amplifiers – including specifically the low-frequency 1/f type noise – is sufficiently good that fully passive real-time systems are possible without the use of superconducting or other cryogenic sensors.

II. Amplitude-only Active Imaging

Amplitude-only active images is the modality that humans are accustomed to receiving from their retinas and interpreting, whether the illumination source is natural, e.g. sunlight, or artificial, e.g. incandescent lamps, flashlights, oil lamps, etc. Therefore, it is logical that THz imaging systems that use active illumination should operate in the same mode. However, it is important to note that virtually all of these systems employ coherent sources, e.g. multiplied mm-wave sources or quantum cascade lasers, as illumination, for the simple reason that these are by far the strongest THz sources available.

One important question is the degree to which the surfaces behave as Lambertian scattering surfaces. It has been recognized for many years that real-world surfaces scatter more specularly at the low end of the frequency band (say 100 GHz) and more diffusely, i.e. closer to a Lambertian surface, at the upper end (say 1000 GHz)[5]. Well known phenomenology treatments of THz imaging[6, 7] have dealt with this in rather crude fashion, either demanding a user-input superposition of purely specular and purely Lambertian components, or assuming a purely Lambertian dependence respectively, mainly because very few quantitative measurements exists on THz scattering and its angular dependence. We have constructed two goniometer-based setups to measure this bistatic scattering, covering the frequency range from 160-650 GHz. Both perform measurements of bi-directional reflectance distribution (BRDF), which is equivalent to normalized radar cross-section. The first set of samples measured was a sequence of

ten artificial rough surfaces constructed by mixing various sizes of Al_2O_3 grit in an epoxy binder. This was inspired by, and closely followed the construction technique of [8], in which diffusely scattering, absorptive coatings were developed to suppress stray light in the HIFI and PACS instruments for Herschel. The roughness levels embodied inour samples cover a range of approximately 25 – 300 µm, i.e. $0.014 \le \sigma/\lambda \le 0.65$ for frequencies of 160 – 650 GHz. To obtain accurate quantitative information on the roughness of these and other samples, focus-variation microscopy was performed to obtain full 3-dimensional topography of the surfaces. Examples of this topography are shown in Fig. 1, for one of the rougher and one of the smoother samples in this set.

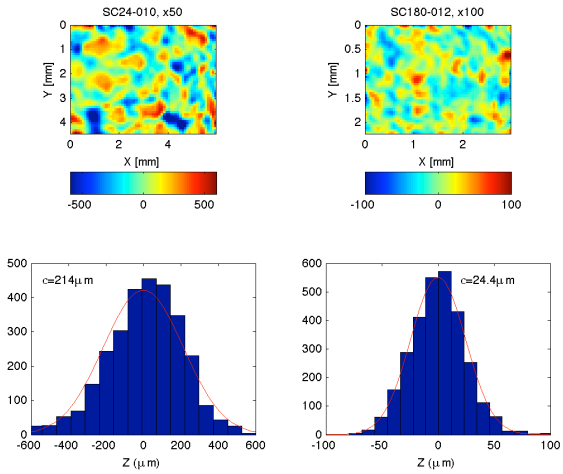

Fig. 1. Surface topography (map and histogram) for two of the ten rough surface scattering targets used in the bistatic measurements, one of the rougher samples on the left and a smoother sample on the right. Note difference in scales.

A. Mean scattered intensity

Scattering from random rough surfaces is a hoary subject in electromagnetic theory. Two limiting cases are well known, the Rayleigh and Kirchoff approximations. The Rayleigh limit lImit is simply $\sigma/\lambda \ll 1$ which clearly does not apply for our samples nor for the vast majority of real-world surfaces in THz images. The Kirchoff approximation is a low-curvature limit, in which fluctuations in elevation are manifested as "rolling hills" rather than "mountainous cliffs", and is numerically described by $\sigma\lambda/L^2 \ll 1$, where L is the autocorrelation length of the surface elevation. This is the most sophisticated theory to have been compared with measurement in the THz regime to date [9], but the approximation also breaks down for a large class (possibly the majority) of realistic surfaces in the THz band. We have adopted an algorithm based on the integral equation method, IEM-B, as described in [10]. These theoretical comparisons (see Figs. 2 and 3) assume that the topography is described by an exponential autocorrelation function with a single length scale (L), and that (as is invariably the case for theoretical treatments) the height fluctuations are described by a Gaussian probability distribution with an RMS level of σ . For both theory and experiment, we describe the diffusely scattered intensity in terms of BRDF, the ratio of scattered *radiance* (in W/m^2 /srad) to incident *irradiance* (in W/m^2), frequently on a dB scale relative to 1 sr^{-1} .)

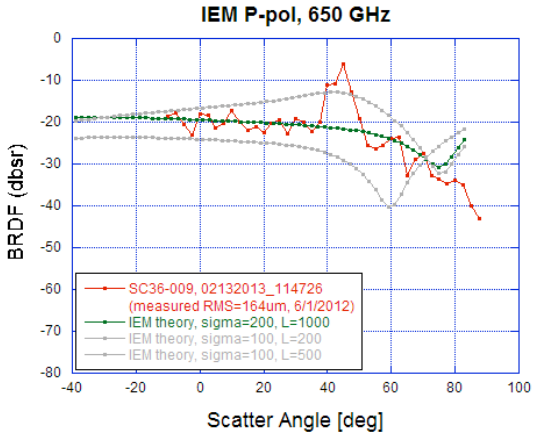

Fig. 2. Measured bistatic scattering on a scattering target with nominally 480 µm diameter grit and measured RMS surface roughness of 164µm. Green trace is the IEM-B theory prediction with RMS roughness of 200 µm and 1000 µm autocorrelation length. Grey traces are theoretical curves for differing roughness parameters.

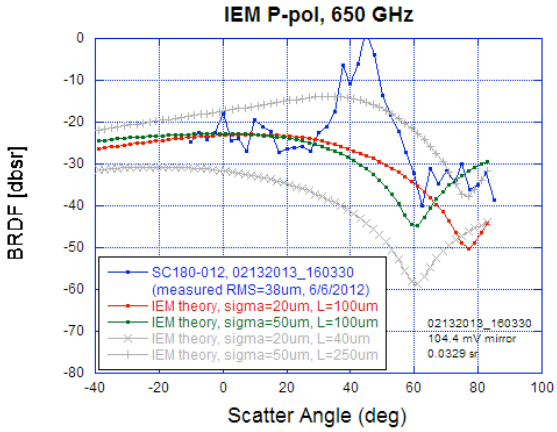

Fig. 3. Measured bistatic scattering on a scattering target with nominally 60 µm diameter grit and measured RMS roughness of 38 µm. Red, green and gray traces are IEM-B theory, the best fit falling between the red and green parameters

.

Figures 2 and 3 display the diffuse scattering measured at 650 GHz on a relatively rough and relatively smooth sample respectively, at an incidence angle of -45°, in p-polarization. The former sample has nearly the same roughness level as the sample in 1a; the latter sample is the same one whose topography is displayed in Fig. 1b. Scatter angle is measured

from the sample normal, so specular reflectance occurs at a scatter angle of +45°. The IEM theory only treats diffuse scattering, so a large specular peak is expected in the measurements (for smoother samples) that is not included in the theory. An extremely important point is that there are no free parameters in the IEM theory. The theoretical traces shown in Figs. 2 and 3 have not been adjusted with an arbitrary multiplicative factor. Because this measurement was performed in p-polarization, the IEM theory predicts a marked dip at a scattering angle close to (but not exactly at) the Brewster angle. We have broadened this dip in the theoretical plots by an amount corresponding to the actual angular resolution of the measurement setup. For both of these samples, it is clear that the IEM theory is remarkably accurate in predicting the diffusely scattered THz radiation. The matching theoretical trace for the rougher sample corresponds to an RMS roughness of 200 μm, quite close to the 164 μm value measured from the topography, and an autocorrelation length of 1 mm. The matching theory for the smoother sample likewise falls between an RMS roughness of 20 μm and 50 μm, in agreement with the 38 μm value measured from the topography, and an autocorrelation length of 100 μm..

B. Speckle

It is apparent in Figs. 2 and 3 that the scatter measurements, while centered around the mean scattered intensity given by IEM theory, display large fluctuations in intensity about that mean. Moreover, the ratio of the fluctuations to the mean, often described as the contrast $C = \sigma_I / \bar{I}$, does not improve when the mean intensity increases, even by a factor of several dB, as it does between Fig. 3 and Fig. 2. This is a characteristic property of speckle phenomena, which arise when the illumination incident on a surface is coherent[11]. These phenomena have been extensively studied in the visible region since the invention of the laser, and have a similarly long history in the microwave region. The fundamental result related to intensity fluctuations (§3.2 of [11]) is that in fully developed speckle, the probability distribution for the intensity is a negative exponential, not a Gaussian (as it would be for incoherent illumination). The resulting contrast $C = 1$, independent of the mean scattered intensity, and the ratio of median to mean intensity is $\ln(2)$, again independent of the mean intensity. These fluctuations have a major impact on the ability of the eye to discern patterns in the resulting images, i.e. on the effective spatial resolution.

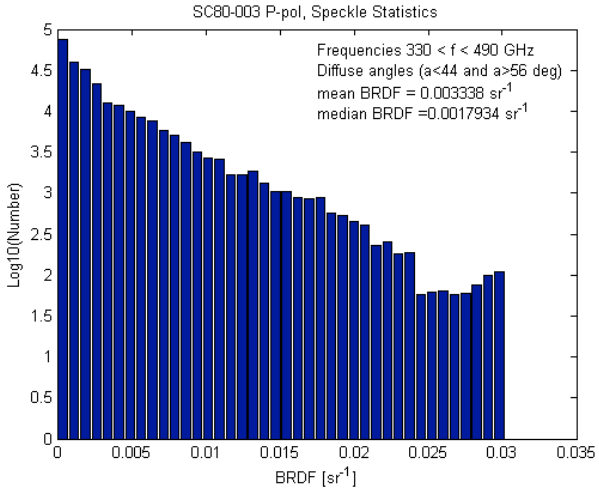

Fig. 4. Distribution of measured bistatic BRDF measurements ona sample with nominally 170 μm diameter grit.

Fig. 4 displays the distribution of scattered intensity from another, intermediate roughness, sample from the same set. This histogram includes all measurements within a 330-490 GHz passband, and at scatter angles outside the specular range (outside ±6° of the specular angle. Displayed on a logarithmic intensity scale, it clearly exhibits a negative exponential distribution over nearly all the measured range of BRDF. The measured ratio of median to mean scattered intensity is 0.54, not too far from the ln(2)=0.69 value expected for fully developed speckle. The term "fully developed" speckle refers to the RMS variation in path length from surface to sensor relative to a radian, $2\pi\sigma/\lambda$. (In this case, the variation in path length equals the variation in the topographic height of the sample because the incident angle is 45° .) For this particular sample, $\sigma = 55\,\mu m$ and $2\pi\sigma/\lambda_{mean} = 0.47$. The mathematical treatment of partially developed speckle is complex (see §3.5 and appendix B of [11]) but does yield the following simple result. The contrast in intensity fluctuations begins at 0 for perfectly smooth surfaces and increases with $2\pi\sigma/\lambda$, reaching the fully developed limit (C=1) by the time $2\pi\sigma/\lambda \geq 0.3$ in all cases. We therefore conclude that, for the rough surfaces embodied in these targets, IEM theory provides a good estimate of the mean scattered intensity as a function of angle, while the fluctuations in scattered intensity are well described by speckle theory, varying from partially developed speckle for the smoothest samples but reaching the fully developed limit even for surfaces of only moderate roughness.

III. PASSIVE IMAGING

The degradation in THz images caused by speckle can be addressed in various ways, for example adding angular diversity [12] or multimode mixing[13] to the illumination source. A simpler alternative is adoption of a fully passive approach, which in many applications has additional advantages of stealth, regulatory requirements, or public acceptance related to health concerns. A fully passive approach requires a very challenging level of sensitivity however, that until recently has only been attainable with cryogenically cooled sensors or with heterodyne receivers. Arrays of cryogenic sensors operating at 4K, 0.3 K, or even lower temperature, have been adapted from astronomical receivers and explored for real-world (terrestrial) applications [14-17], but their drawbacks in terms of size, weight, power, reliability, and cost are obvious. On the other hand, in the last five years, major advances have been made in terahertz monolithic (and therefore array-compatible) integrated circuits [18], often called TMICs, operating at room temperature.

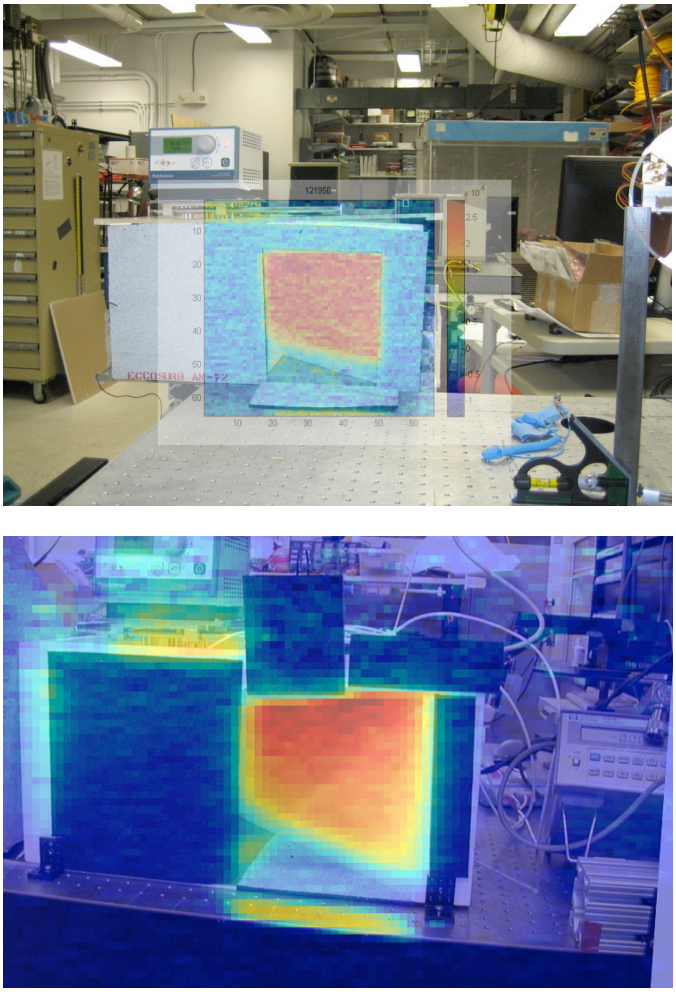

Fig. 5. Passive submm images of the NIST ABC source. (Top) image taken with a broadband 4K microbolometer[14] (Bottom) image taken with the NGAS 650 GHz LNA coupled to a zero-bias diode.

Good low-noise (LNA) and power amplification is now possible as high as 650 GHz[19] using InP HEMT and HBT transistors. Their performance for passive imaging is described by noise-equivalent temperature difference (NETD). Although this is nominally determined by an (equally weighted) combination of noise figure and bandwidth, less commonly addressed issues of gain stability, 1/f noise, and input-coupling loss are also critical.

To address the usefulness of InP TMICs for fully passive imaging, we have combined samples of Northrup-Grumann's recently developed 650 GHz LNAs with commercial zero-bias diodes, in a configuration similar to the W-band passive imaging chipset developed by HRL in 2008[20]. An image taken by raster scanning a single pixel across the exit aperture of a NIST Aqueous Blackbody Calibration (ABC) source is shown in Fig. 5. The ABC source, which is actually optimized for the 200-400 GHz range, presents an accurate 60C radiometric temperature (against a 20C ambient temperature) within a specified aperture and field-of-view, and was developed specifically for performance testing (i.e. NETD measurement) of passive imagers[21]. The image taken with the NGAS amplifier is compared directly to an image taken in 2007 with a cryogenic (4K) hotspot microbolometer. The qualitative similarity of the image quality is readily apparent. Quantitative analysis of the NETD is ongoing; at present NETD is limited by 1/f noise rather than the LNA's fundamental noise figure.

IV. Conclusion

We have presented selected measurements of 325-650 GHz bistatic scattering from rough surfaces. The roughness levels, 25 – 300 μm, correspond well to the levels encountered for everyday surfaces, both natural and manufactured, appearing in scenes of interest for many THz applications. The mean intensity levels for bistatic scattering agree well, in angular dependence and absolute level, with predictions of the IEM-B theory. The fluctuations about the mean intensity appear to agree with the theory of fully developed speckle.

A simple passive imaging demonstration has also been made, showing that the image quality available by using existing uncooled InP HEMT LNAs as the front end sensor is very comparable to that available by using a cryogenically cooled (4K) superconducting hotspot bolometer as the sensor. This has substantial implications for the future development practical applications of passive THz imagers.

Acknowledgment

We are very grateful to William Deal, Kevin Leong, and others at Northrup-Grumann Aersopace Systems for providing the 650 GHz LNAs. Their development was sponsored by the DARPA Terahertz Electronics Program. The scattering studies were sponsored by the Dept. of Homeland Security under a program on Phenomenology and Modelling of Submillimeter Imaging.

References

[1] P. H. Siegel, "Terahertz Technology," *IEEE Trans. Microwave Theory and Tech.*. vol. 50, pp. 910-928, 2002.

[2] K. B. Cooper, R. J. Dengler, N. Llombert, B. Thomas, G. Chattopadhyay, and P. H. Siegel, "Terahertz Imaging Radar for Standoff Personnel Screening," *IEEE Trans. THz Sci. Tech,* vol. 1, pp. 169-182, 2011.

[3] Z. D. Taylor, R. S. Singh, D. B. Bennett, P. Tewari, C. P. Kealey, N. Bajwa*, et al.*, "THz Medical Imaging: in vivo Hydration Sensing," *IEEE Trans. THz Sci. and Applic.,* vol. 1, pp. 201-219, 2011.

[4] F. Friederich, W. Von Spiegel, M. Bauer, F. Meng, M. D. Thomson, S. Boppel*, et al.*, "THz Active Imaging Systems with Real-time Capabilities," *IEEE Trans. THz Sci. and Applic.,* vol. 1, pp. 183-200, 2011.

[5] N. A. Salmon, and and P. R. Coward, "Scattering in Polarimetric Millimetre-wave Imaging Scene

Simulation," *Proc. SPIE,* vol. 6211, pp. 6211071-8, 2006.

[6] S. R. Murrill, Jacobs, E.L., Moyer, S.K., Halford, C.E., Griffin, S.T., DeLucia, F.C., Petkie, D.T., Franck, C.C., "Terahertz Imaging System Performance Model for Concealed-weapon Identification," *Appl Optics,* vol. 47, pp. 1286-1297, 2008.

[7] H. B. Wallace, "Analysis of RF Imaging Applications at frequencies over 100 GHz," *Appl Optics,* vol. 49, pp. E38-E47, 2010.

[8] T. O. Klaassen, J. H. Blok, J. N. Hovenier, G. Jakob, D. Rosenthal, and , and K. J. Wildeman, "Scattering of Submillimeter Radiation from Rough Surfaces: Absorbers and Diffuse Reflectors for HIFI and PACS," *Proc. SPIE, "IR Space Telescopes and Instruments",* vol. 4850, pp. 788-791, 2003.

[9] C. Jansen, S. Priebe, C. Moeller, M. Jacob, H. Dierke, M. Koch*, et al.*, "Diffuse Scattering from Rough Surfaces in THz Communications Channels," *IEEE Trans. Terahertz Sci. and Applic.,* vol. 1, pp. 462-472, 2011.

[10] A. K. a. Fung and K. S. Chen, *Microwave Scattering and Emission Models for Users*. Norwood, MA: Artech House, 2010.

[11] J. W. Goodman, *Speckle Phenomena in Optics*. Greenwood Village, CO: Roberts and Co., 2007.

[12] A. Luukanen, Miller, A.J., Grossman, E.N., "Active millimeter-wave video rate imaging with a staring
120-element microbolometer array," *Proc. SPIE,* vol. 5410, pp. 195-201, 2004.

[13] M. A. Patrick, J. A. Holt, C. D. Joye, and F. C. DeLucia, "Elimination of Speckle and Target Orientation Requirements in Millimeter-wave Active Imaging by Modulated Multimode Mixing Illumination," *J. Opt. Soc. Am. A,* vol. 29, p. 2643, 2012.

[14] A. Luukanen, E.N. Grossman, A.J. Miller, P. Helist¨o, J.S. Penttil¨a, H. Sipola, and H. Sepp¨a, "An Ultra-Low Noise Superconducting Antenna-Coupled Microbolometer With a Room-temperature Read-out," *IEEE Microwave and Wireless Components Letters* vol. 16, pp. 464-466, 2006.

[15] Grossman E.N., C. Dietlein, J. Ala-Laurinaho, M. Leivo, L. Gronberg, M. Gronholm*, et al.*, "Passive Terahertz Camera for Standoff Security Screening," *Appl. Optics,* vol. 49, pp. E106-E120, 2010.

[16] E. Heinz, T. May, G. Zieger, D. Born, S. Anders, G. Thorwith*, et al.*, "Passive Suibmillimetyer-wave Stand-off Video Camera for Security Applications," *Int. J. Infrared Milli Terahz Waves,* vol. 31, pp. 1355-1369, 2010.

[17] D. Becker, C. Gentry, P. Ade, J. Beall, H.-S. Cho, S. Dicker*, et al.*, "High-resolution Passive Video-rate Imaging at 350 GHz," *Proc. SPIE,* vol. 8022, pp. 802206-1 - 802206-9, 2011.

[18] W. Deal, X. B. Mei, M. K. H. Leong, V. Radisic, S. Sarkozy, and R. Lai, "THz Monolithic Integrated Circuits using InP High Electron Mobility Transistors," *IEEE Trans. Terahertz Sci. and Applic.,* vol. 1, pp. 25-32, 2011.

[19] V. Radisic, M. K. H. Leong, X. Mei, S. Sarkozy, W. Yoshida, and W. R. Deal, "Power Amplification at 0.65 THz using InP HEMTs," *IEEE Trans. Microwave The. and Tech.,* vol. 60, pp. 724-729, 2012.

[20] J. J. Lynch, H. P. Moyer, J. H. Schaffner, Y. Royter, M. Sokolich, B. Hughes*, et al.*, "Passive Millimeter0wave Imaging Module with Preamplified Zero-bias Detection," *IEEE Trans. Microwave Theory and Tech.*. vol. 56, pp. 1592-1600, 2008.

[21] C. R. Dietlein, Z. Popovic, and E.N. Grossman, "Aqueous Blackbody Calibration Source for Millimeter-wave/Terahertz Metrology " *Appl Optics,* vol. 47, pp. 5604-5615, 2008.